An Integrated Macro/Micro Approach to Evaluating Pivot Flow Within the Medtronic ADVANTAGE™ Bileaflet Mechanical Heart Valve

Mark C. S. Shu[1], Jeffery M. Gross[1], Keith K. O'Rourke[2], Ajit P. Yoganathan[3]

[1]Medtronic Heart Valves, Inc., Santa Ana, CA, USA, [2]Adaptive Research Inc., Alhambra, CA, USA, [3]Georgia Institute of Technology, Atlanta, GA, USA

Background and aim of the study: **An integrated macro/micro approach was used to evaluate flow within the pivots of the Medtronic ADVANTAGE™ bileaflet heart valve. Results were compared with those obtained with the St. Jude Medical® bileaflet heart valve.**

Methods: **The integrated macro/micro approach consists of both a macroscopic hydrodynamic performance assessment and a three-part microscopic flow analysis. The hydrodynamic performance assesses the basic dynamic functions of the valves, while the microscopic flow analysis uses pivot flow visualization, computational fluid dynamics and laser Doppler velocimetry to determine pivot flow characteristics. Pivot flow visualization captures two-dimensional images of the pivot flow, defines the computational fluid dynamics boundary conditions, and validates the computational result. Three-dimensional unsteady computational fluid dynamics simulation reconstructs pivot flow structures. Laser Doppler velocimetry maps pivot velocity field and provides velocity validation for the computational simulation.**

Results: **The macroscopic hydrodynamic performance assessment showed the ADVANTAGE and St. Jude Medical valves to be comparable under identical flow conditions. The three techniques in the microscopic analysis mutually confirmed that the pivot design of the ADVANTAGE valve permits continuous-flow washing in the pivot recess, the pivots of both valves are completely wiped twice in a cardiac cycle, and no persistent pivot flow stases are observed.**

Conclusion: **The integrated macro/micro approach represents a powerful systematic method for determining detailed microscopic flow structures inside the pivots of bileaflet mechanical valves. The use of this technique during the design process of a bileaflet valve can eliminate the persistent flow stases that lead to thrombus formation.**

The Journal of Heart Valve Disease 2003;12:503-512

The success of a bileaflet mechanical heart valve depends on the absence of persistent flow stases that may cause thrombus formation. Within the valve housing, the only obstruction to blood flow is the leaflets. The leaflet faces are repeatedly washed by blood as the valve opens and closes, but persistent flow stasis can occur at the leaflet pivot due to its size, location and design, as evidenced by recent thrombus-related failure (1-3). Therefore, it is imperative to characterize pivot flow of any bileaflet mechanical heart valve design prior to its clinical use (4).

Pivot flow analysis is complicated by the geometry of the valve and its pivots. In general, a bileaflet mechanical heart valve typically comprises a rigid annular valve housing and a pair of rotatable leaflets (5-9) (Fig. 1). Each leaflet has a pair of ears that protrude from the leaflet and mate with the pivot recesses in the valve housing. The leaflet is retained inside the valve housing by the pivots, which control the range of the leaflet movement as the leaflets respond passively to local blood flow pressure gradients. Pivot flow analysis is challenging because the rotating leaflet obstructs visibility, and the complexity and motion of the pivot region result in complex flow that is difficult to measure or simulate.

The present study outlines a systematic, detailed method for characterizing pivot flow of the Medtronic ADVANTAGE™ (ADV) bileaflet mechanical heart valve. This method, which was used during the design process of the ADV, combines both a macroscopic hydrodynamic performance assessment and a microscopic flow analysis. The St. Jude Medical® (SJM) bileaflet mechanical valve was used as the control in these studies.

Address for correspondence:
Mark CS Shu PhD, Medtronic Heart Valves, 1851 East Deere Ave., Santa Ana, CA 92705, USA

J Heart Valve Dis
Vol. 12. No. 4
July 2003

Design characterization of the ADV and SJM valves

The ADV valve is a low-profile bileaflet mechanical heart valve (Fig. 1). The large radius inflow rim and two large inflow chamfers connecting to the primary flats are designed to guide blood flow into the valve housing at opening (Fig. 2). The central flow orifice between both leaflets is slightly enlarged compared to other bileaflet valves to minimize jet flow contraction (vena contracta) at opening.

The ADV valve employs a bi-level butterfly pivot design. The pivot is bi-level with respect to the pivot neck and consists of a primary flat, a butterfly recess, and a secondary flat, which is recessed slightly compared to the primary flat (Fig. 2). The bi-level butterfly pivot design takes advantage of the minimal forward flow pressure gradient acting on the leaflet faces (Fig. 3) in the construction of the secondary flat (approximate one-third depth into the pivot recess). Lowering the secondary flat from the primary flat level creates a flow channel over the secondary flat for blood, the intention being to reduce flow resistance and promote continuous-flow washing within the pivot recess during each cardiac cycle. Figure 4 provides a comparison between the ADV pivot recess and the SJM pivot recess. The smooth edge radii of the ADV pivot recess may further reduce blood flow resistance comparing to the relatively sharp edge radii of the SJM pivot recess.

The SJM valve is also a bileaflet mechanical valve (see Fig. 2). It has two pivot guards that are extruded towards the inflow side from its housing ring. The SJM pivot consists of a primary flat and a butterfly recess, as indicated by a white broken-line circle in Figure 2. The SJM pivots are located on the pivot guards.

The major design features between the ADV and SJM valves are compared in Table I. The microscopic flow analysis results of both valves are presented and compared on Plane C, as indicated in Figure 3. This plane is adjacent and parallel to the secondary flat.

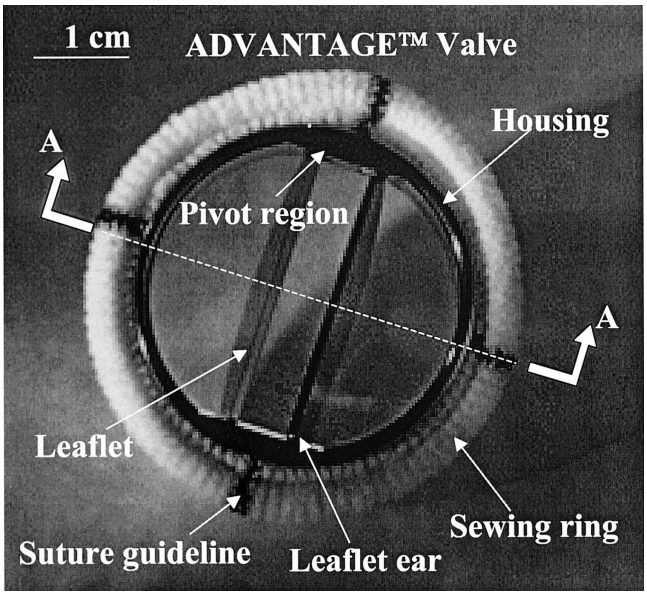

Figure 1: Nomenclatures are defined for a typical bileaflet mechanical valve. The section view (A-A) is used for the ADVANTAGE™ (ADV) and St. Jude Medical (SJM) valves in Figure 2.

Materials and methods

The integrated macro/micro approach consists of a macroscopic hydrodynamic performance assessment and a microscopic flow analysis of the pivot. Both analyses are essential to understand a bileaflet valve's functional performance and ability to resist thrombus formation in its pivots due to regions of persistent flow stasis. The hydrodynamic performance assesses the basic hydrodynamic functions of the ADV and SJM valves. The microscopic flow analysis uses three independent techniques to explore pivot flow characteristics: (i) Pivot flow visualization (PFV); (iii) three-dimensional (3D) unsteady computational fluid dynamics (CFD) simulation; and (iii) laser Doppler velocimetry (LDV). The PFV acquires a two-dimen-

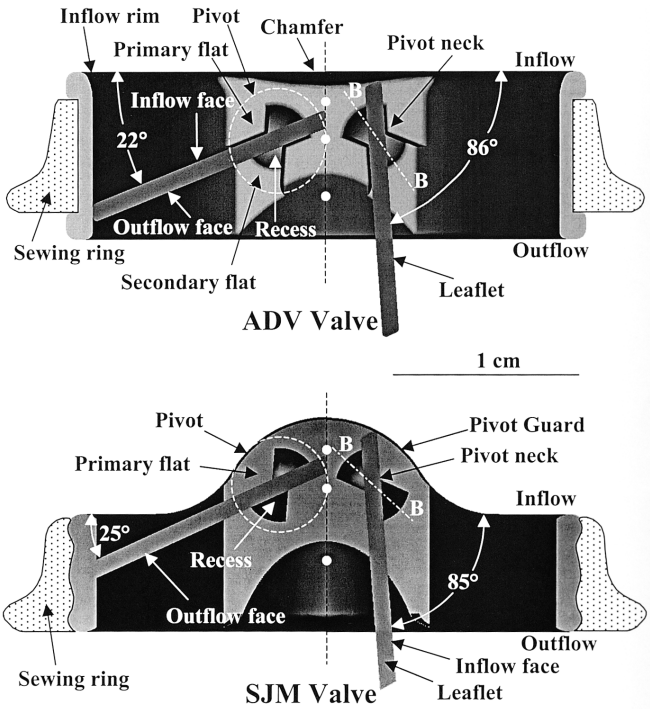

Figure 2: The A-A view of the ADV valve depicts the bi-level butterfly pivot that consists of a primary flat, a recess, and a secondary flat recessed from the primary flat. The pivot is bi-level with respect to the pivot neck. The A-A view of the SJM valve shows the pivot formed from a primary flat and a recess on a pivot guard. The three white dots along the center-line indicate the LDV validation points. Scale bar = 1 cm for both valves.

Table I: Major design feature comparison between ADVANTAGE™ (ADV) and St. Jude Medical® (SJM) valves.

Design feature	ADV	SJM
Material	PyC coated on graphite substrate	PyC coated on graphite substrate
Pivot guard	No	Yes
Central flow orifice	Wider	Conventional
Pivot design	Bi-level butterfly	Butterfly
Secondary flat	Yes	No
Leaflet excursion angles	Open 86°; Closed 22°	Open 85°; Closed 25°
Inflow Chamfer	Yes	No

PyC: Pyrolytic carbon.

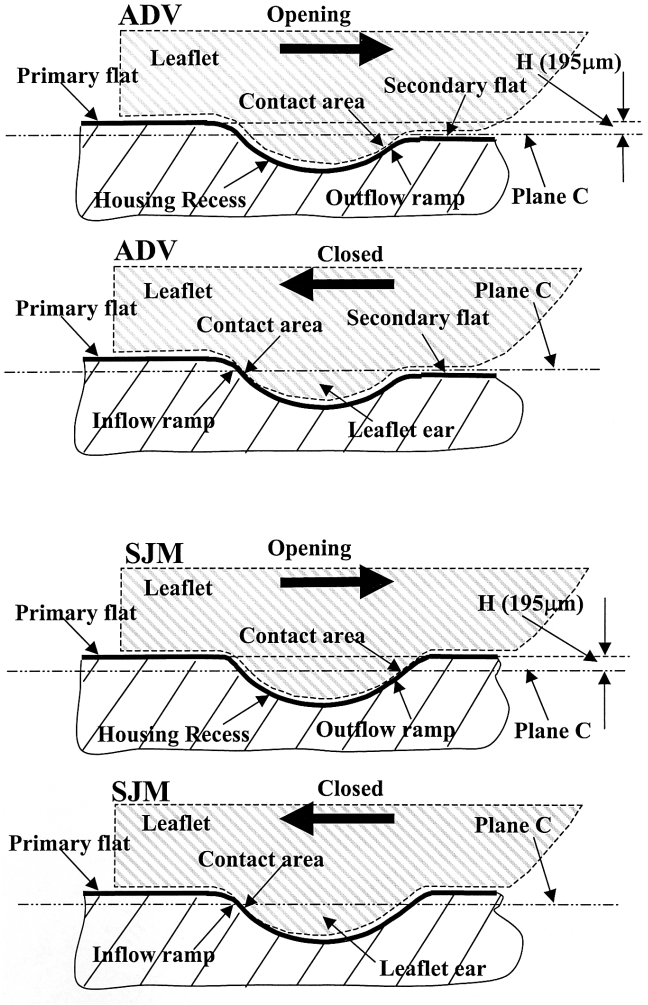

Figure 3: Schematic B-B section views for the ADV and SJM valves. The leaflet contacts the outflow ramp under minimal forward flow pressure gradient at opening and the inflow ramp under large backflow pressure gradient after valve closure for both valves. The ADV's view depicts the location of the secondary flat (approximate one-third depth into the recess). The recessed secondary flat takes advantage of minimal forward pressure gradient and provides easy access for blood. Plane C is at the distance of H away from the primary flat.

sional image of the microscopic flow field, defines the CFD flow boundary conditions, and validates the CFD result. The CFD simulation calculates and reconstructs pivot flow structures. The LDV maps the pivot velocity field and provides velocity validation for the CFD simulation. The results of these three techniques are compared to validate each other.

Macroscopic hydrodynamic performance

The macroscopic hydrodynamic performance assessment of the ADV and SJM valves was conducted as per the FDA's Replacement Heart Valve Guidance (10) and ISO 5840 (11) in both the mitral and aortic positions using three of each ADV valve tissue annulus diameter (19, 21, 23, 25, 27 and 29 mm) and two SJM reference valves (21 and 29 mm). According to the FDA's Guidance and ISO 5840, only one aortic reference valve and one mitral reference valve of any tissue annulus diameter are required and tested under identical conditions to establish hydrodynamic equivalency between the test valve and the reference valve.

The assessment was performed using a pulse dupli-

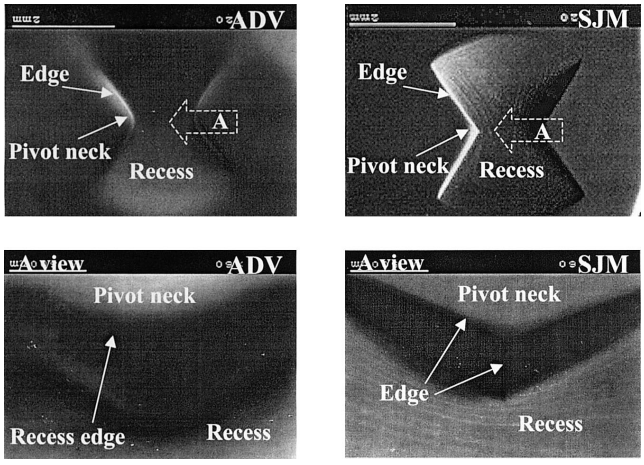

Figure 4: Enlarged views of the ADV and SJM pivot recesses show that the ADV valve has larger and smoother recess edge radii than the SJM valve.

J Heart Valve Dis
Vol. 12. No. 4
July 2003

cator capable of producing physiological pressure and flow waveforms. The duplicator consists of an open left atrial chamber, an elastic left ventricle in a sealed chamber, an elastic aorta with molded sinuses of Valsalva, two compliance chambers, and two flow resistors. The motion of the left ventricle is controlled via a voice coil motor connected to a PC computer (Compaq Deskpro) that follows a left ventricular volume curve. A schematic view of the pulse duplicator's left atrium, mitral valve, and left ventricular chamber is shown in Figure 5. Similar duplicators have been reported by other investigators (12-14). The test was conducted at a cardiac rhythm of 70 beats/min (bpm) with four cardiac outputs (2, 3.5, 5 and 7 l/min) and aortic pulse pressure of 120/80 mmHg. For dynamic regurgitation, the range of cardiac rhythm was 45 to 120 bpm. The test fluid used was physiological saline.

Three pressure waveforms (atrial, ventricular, and aortic) and two flow rate waveforms (mitral and aortic) were acquired during the test. The pressures were measured using Cobe pressure transducers (Model #041-500-503; Cobe, Lakewood, CO, USA) connected to Gould transducer amplifiers (Model #13-4615-50; Gould Inc., Valley View, OH, USA). The flow rates were monitored using two electromagnetic flow meters and two flow probes (Model # EP672P1; Carolina Medical Products, King, NC, USA). All waveforms were digitized at a sampling rate of 250 Hz per channel using a PC-based analog/digital data acquisition system (Model #PCI-MIO-16E-1; National Instruments, Austin, TX, USA) and analyzed using custom software developed with LabView (Version 5.1, National Instruments). The pulsatile pressure drops and dynamic regurgitation were calculated for each cycle and averaged over ten consecutive cardiac cycles.

Microscopic flow analysis

For the microscopic flow analysis, the 29 mm mitral ADV and SJM valves were compared. This selection was made as it represented the most challenging condition for both designs. In the mitral position, only a minimal pressure gradient drives flow through the valve, causing low forward flow velocities both in the bulk flow field and in the pivots.

Pivot flow visualization

PFV qualitatively characterizes the flow fields immediately adjacent to and within the pivots of the ADV and SJM valves. The PFV images were captured using a clear valve model. The model housing was directly fabricated from the ADV valve's housing using transparent epoxy resin. The clear valve housing had fine platinum wires (diameter 100 μm) half-embedded into the primary flat surface immediately proximal and distal to the pivots. These wires, which protrude radially inward <50 μm, act as sources for hydrogen bubble generation. The leaflets were fitted into the clear housing made from that valve's pyrolytic carbon (PyC) housing. The identical procedure was also used to fabricate a clear valve model of the SJM valve.

PFV was conducted in the mitral position of the pulse duplicator. A minor modification was carried out at the mitral valve mounting site to accommodate the clear valve model. The test conditions were identical to those used in the hydrodynamic performance, with the exception that a single cardiac output (4 l/min) was used. The test fluid was a mixture of glycerin and normal saline with a viscosity of 3.5 cP and a density of 1.1 g/ml at room temperature. The valve pivots were illuminated with a white-light beam. The flow structures immediately adjacent to and within the pivots were discerned by recording hydrogen bubble streak lines

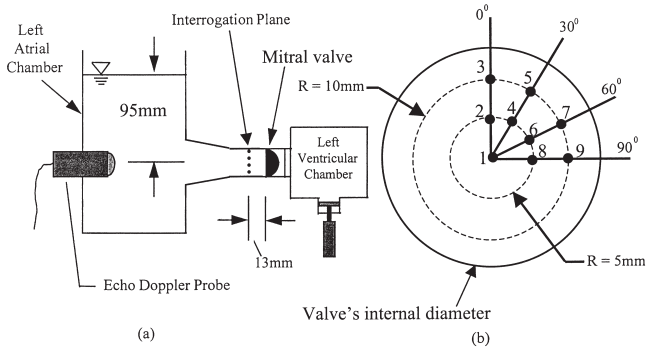

Figure 5: A schematic diagram of the pulse duplicator's left atrium, mitral valve, and left ventricular chamber shows the location of the echo-Doppler velocity interrogation plane proximal to the mitral valve (a) and the arrangement of the measuring points on the plane (b). The horizontal line (90°) matches the A-A cut-away line in Figure 1.

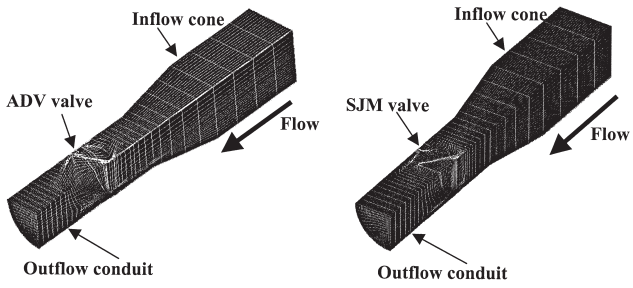

Figure 6: Each quarter CFD models consists of a truncated inflow cone, a valve, and an outflow conduit. A coarse CFD cell mesh is used in the cone and in the conduit, whereas a fine cell mesh is used inside the valve housing and in the pivot region.

using a Kodak EktaPro Motion Analyzer (Model 2000; Eastman Kodak Co, San Diego, CA, USA) set at 1,000 frames per second.

PFV provides flow boundary conditions and macroscopic velocity validation for the CFD simulation. These conditions include a time-dependent mass flow rate waveform and a time-dependent leaflet motion. An HP Sonos 1000CF echo-Doppler system (Hewlett-Packard Co., Andover, MA, USA) was used to measure echo-Doppler velocity profiles at nine points on an interrogation plane located 1.3 cm proximal to the valve (Fig. 5). These velocity profiles validate the macroscopic velocity field calculated in the CFD simulation.

CFD simulation

The 3D unsteady CFD model simulates blood flow through a flow domain. The simulations of the 29 mm ADV and SJM valves were conducted at the mitral position using the CFD code CFD2000 STORM (Adaptive-research, Alhambra, CA, USA). The CFD models were created based on the design geometry file of the ADV valve and the measured coordinate measuring machine dimensions of a clinical SJM valve. Because of the symmetry of a bileaflet valve design, the CFD model was created using only one-quarter of the valve housing. The model consisted of a truncated inflow cone, the valve, and the outflow conduit (Fig. 6). The domain was divided into a number of cells (volume grids), with each cell being constructed using the technique of transfinite interpolation. A total of approximately 40,000 cells for each model was generated using variable cell mesh. A coarse cell mesh was used in the cone and the conduit, whereas a fine cell mesh was used inside the valve housing and pivot region.

To simulate valve leaflet motion through a cardiac cycle, the CFD simulation incorporated a 3D moving cell technique. The full Navier-Stokes equations were solved using a finite volume method with a pressure-based algorithm for continuity, and a Pressure-Implicit with Splitting of Operators algorithm for pressure-velocity coupling. During the simulation, the full Navier-Stokes equations were calculated twice in

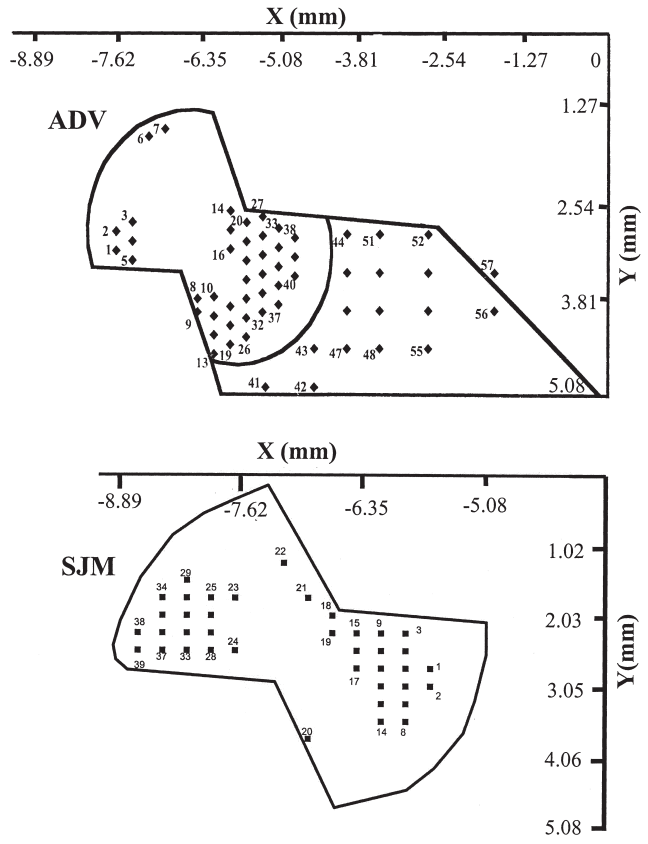

Figure 7: A schematic presentation of the LDV measurement points on the Plane C (see Fig. 3). The blank areas in the recesses are lack of LDA measurement. The X- and Y-axes are parallel to the center-line and the inflow rim in Figure 2, respectively.

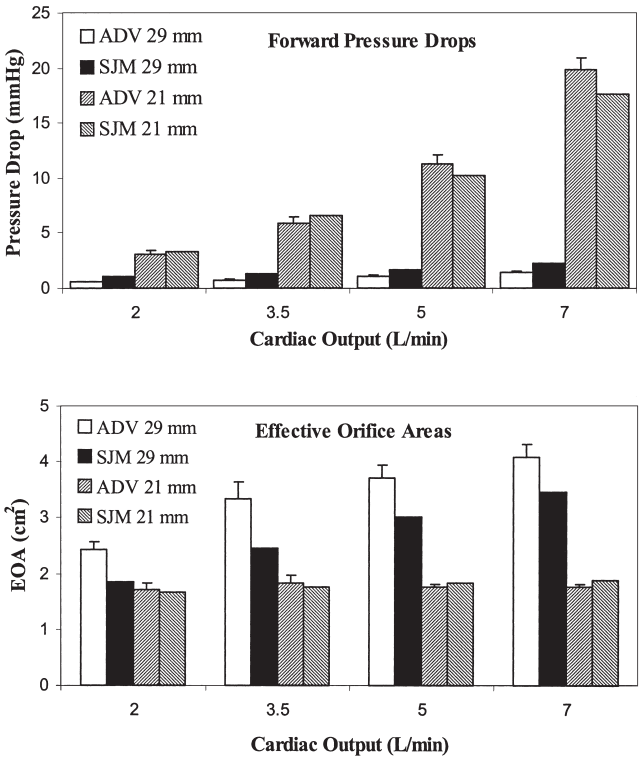

Figure 8: The macroscopic hydrodynamic performance results reveal that the 29 mm mitral ADV valve has statistically lower pressure drops and higher effective orifice area (EOA) values than the 29 mm SJM valve, while the results for both aortic 21 mm valves are statistically comparable. Each bar for the ADV represents a mean value for three valves.

J Heart Valve Dis
Vol. 12. No. 4
July 2003

order to eliminate any potential acceleration errors imposed on the pressure and flow fields at the beginning of the valve opening. The initial flow and pressures inside the flow domain were set to zero for the first simulation run. The final flow and pressure distributions from the first simulation run were used as the initial flow and pressure conditions for the second simulation run. Due to the leaflet rotation in a cardiac cycle, the computational flow domain became complicated, and careful cell arrangement was carried out to avoid cell skewing or tangling before and after cell movement.

The flow boundary conditions for the CFD simulations were derived experimentally as part of the PFV. The time-dependent mass flow rate was applied uniformly to the inlet cross-section surface of the CFD model, while zero pressure was fixed at the outlet surface since only the pressure gradient is relevant to the problem under consideration. Symmetric boundary flow conditions were applied on the planes of symmetry along the axial direction. The leaflet motion measured in the PFV was supplied as a prescribed leaflet movement boundary condition in the simulation.

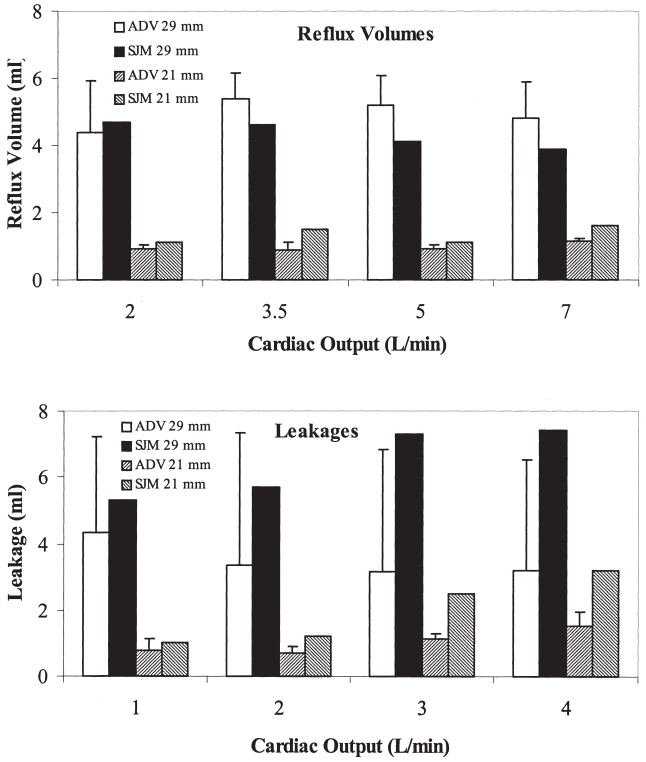

Figure 9: Dynamic regurgitation includes a reflux volume and a leakage volume. The leakage volume is the sum of the leakages through the pivot recesses and the gaps between the leaflets and valve housing. The reflux volumes for both valves are statistically comparable, while the SJM valve exhibits a statistically higher leakage volume. Each bar for the ADV represents a mean value for three valves.

LDV measurements

LDV measures point velocities and, in the present study, was conducted at predetermined points within the pivots of the clear valve models. Figure 7 shows a typical measuring arrangement on Plane C defined in Figure 3. There were some blank areas in the recesses wherein LDV measurements could not be conducted because the rotating leaflet interfered with the Doppler beams.

The microscopic validation between LDV and CFD was conducted at three preselected points which were located 1 mm away from the primary flat surface along the centerline (see Fig. 2). The validation compared the point velocity profiles measured by LDV and calculated by CFD.

The LDV measurement used a blood analog fluid of 79% saturated sodium iodide, 20% glycerin, and 1% water by volume. Silicone carbide particles of diameter 1.5 μm (TSI Incorporated, Minneapolis, MN, USA) seeded the flow to enhance Doppler signals. The kinematic viscosity of the fluid was controlled at 3.5 cSt to match that of blood at physiologic shear rates.

A fiber-optic, three-component, coincident LDV system (Aerometrics Inc., CA, USA) was used to perform two-component velocity measurements. Two focal pairs, green (514.5 nm wavelength) and blue (488 nm wavelength), were formed by color separation of the original laser beam. A 40 MHz frequency shift in one beam for each focal pair was employed to measure reversed flow velocity. The ellipsoidal measuring sample volume produced by the focal pair had major and minor axes of ~140 μm and 21 μm, respectively. Doppler signals generated by the silicon particles

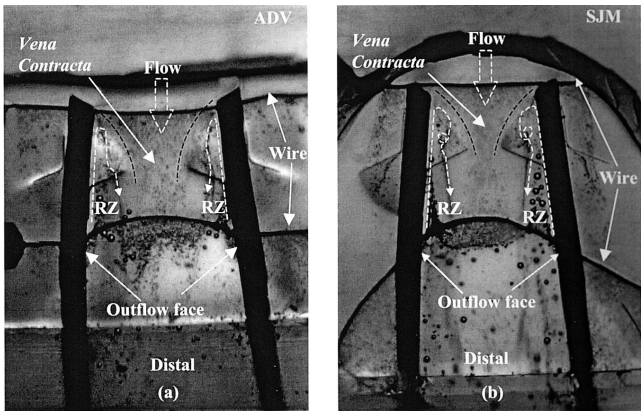

Figure 10: In mid-diastole (184 ms), a smaller vena contracta jet is shown between the SJM valve leaflets. Successive video images show that large bubbles accumulated in the recirculation zone (RZ) slowly recirculate toward the pivot recess. Small vortices can be seen in the SJM valve pivot recesses (white curved broken lines).

through the sample volume were processed using Fast Fourier Transform (FFT)-based real-time signal analyzers. All measurements were conducted in the backscatter mode. Turbulent shear stress was also measured using LDV and determined with a decomposition technique that separated the velocity fluctuation, u′ and v′, from the mean flow velocity.

Results

Macroscopic hydrodynamic performance

The typical hydrodynamic performance results were compared at size 21 mm and 29 mm between the ADV and SJM valves (Figs. 8 and 9). Figure 8 shows forward pressure drop and calculated effective orifice area (EOA) for each tested cardiac output. Each mean value of the ADV valve was averaged from the results of three ADV valves having the same annular diameter. Using the paired *t*-test (a p-value of 0.05 was statistically significant), the results from Excel 2000 (p = 0.0008) showed that the 29 mm SJM mitral valve had a statistically higher forward flow pressure drop and lower EOA than the ADV in this test, while the results for the 21 mm aortic valves were comparable (p = 0.224). Figure 9 presents the dynamic flow regurgitations, the combination of reflux volume and leakage volume. The reflux volume is the fluid volume swept by the leaflet as it swings from its open position toward its closed position. The leakage is the sum of the leakages through the pivot recesses and the gaps between the leaflets and valve housing after the valve is closed. Using the same *t*-test, reflux volumes for both valves were comparable (p = 0.1459), while the SJM valve exhibited a statistically higher leakage volume (p = 0.0168).

Microscopic flow analysis

PFV

PFV images were captured at a total of 857 frames per cardiac cycle for three consecutive cycles. The sequential frames can be analyzed frame by frame at 1-ms intervals. For both valves, the PFV images indicated that the leaflet ear completely wiped the pivot recess twice in each cardiac cycle. The mechanical wiping disrupts microscopic flow structures and expels hydrogen bubbles from the pivot regions.

Figure 10 presents a typical image at 184 ms after the onset of diastole. Hydrogen bubbles emanate from charged platinum wires located proximally and distally to the pivots. Those bubbles are carried distally from the wires by the flow stream. The streak lines in Figure 10 indicate a vena contracta in the central flow orifice between the leaflets. The narrower central orifice of the SJM produces a smaller vena contracta with higher velocity. Flow boundary separation creates large flow recirculation zones along the leaflet outflow faces. The sequential PFV images confirmed that bubbles within these zones recirculate slowly toward the pivot recesses. Small vortices could also be observed within the SJM's pivot recesses (as indicated by the white curved broken lines).

Figure 11 shows single pivot views also taken 184 ms after the onset of diastole from a different cardiac cycle. Sequential images revealed that small bubbles within the SJM's pivot recess move slowly from the inflow face toward the outflow face through the gap between the leaflet ear and the recess bottom (white curved block arrow). A small vortex (indicated by a white

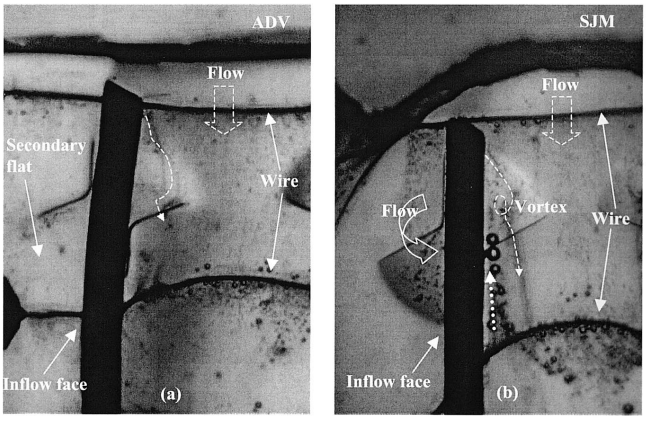

Figure 11: A single pivot image in mid-diastole (184 ms) from a different cycle provides a detailed view of the recess, and reveals better flow washing and a relative clean recess for the ADV valve (a) compared to the SJM valve. Sequential images show that bubbles move slowly from the inflow face toward the outflow face (white curved block arrow) through the gap between the leaflet ear and the recess bottom (b).

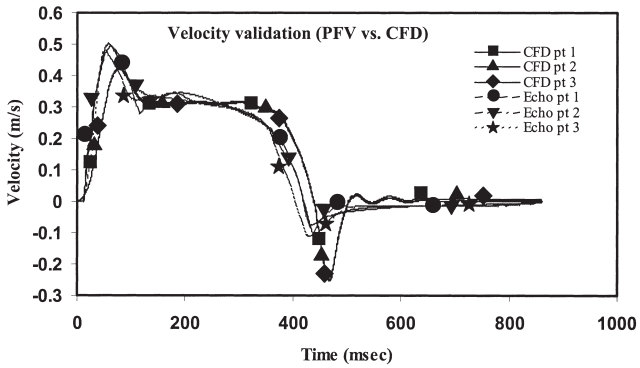

Figure 12: A typical macroscopic comparison is performed between the echo-Doppler velocities and the CFD velocities at Points 1 to 3 on the interrogation plane of the flow domain proximal to the ADV valve (see Fig. 5). The measured and calculated velocities closely resemble each other in terms of velocity magnitudes and profile shapes in a cardiac cycle.

J Heart Valve Dis
Vol. 12. No. 4
July 2003

curved broken line) forms within the SJM's pivot recess. The sequential images indicated that this vortex forms during opening and vanishes when the leaflet swings to closure. In contrast, continual-flow washing occurs at the secondary flat of the ADV. This washing expels small bubbles from the pivot recess and keeps the recess relatively clean with the absence of vortices (Fig. 11a) compared to the SJM's pivot recess.

CFD simulation

CFD simulation provides qualitative as well as quantitative information in a flow domain. Figure 12 depicts a typical comparison between the echo-Doppler velocity profiles obtained in the PFV and the CFD velocity profiles at three points on the interrogation plane defined in Figure 5. The measured and calculated velocities closely resembled each other in terms of magnitude and profile shape in a cardiac cycle. This comparison validated the velocity distribution in the flow domain.

The microscopic validation between the CFD simulation and the LDV measurement was conducted using point velocity at or adjacent to the pivot region of each valve. Figure 13 provides a typical comparison between the calculated velocity profiles and the measured velocity profiles for the ADV valve. The comparison revealed a general agreement in terms of profile shapes and magnitudes, and validated the velocity distribution in the pivot regions between the CFD simulation and the LDV result.

CFD simulation is displayed as sequential frames in Figure 14. These frames are acquired at Plane C (see Fig. 3). The length and direction of velocity vectors designate the magnitude and direction of flow at that point. Valve symmetry permits the calculated result from the quarter valve to be mirror-imaged into a half-valve image for better visualization.

Figure 14 presents typical flow velocity distributions during valve opening and closing on Plane C and highlights potential important differences between the ADV and SJM valves. When the leaflets wiped the pivot recesses during their opening, flow washing was seen through the channel created by the secondary flat of the ADV valve (Fig. 14a). By contrast, the velocity vectors of the SJM valve were shorter, indicating less flow washing (Fig. 14b). When fluid flowed freely through the open valve orifices in mid-diastole, a gentle washing flow (small velocity vectors) persisted through the pivot recesses of the ADV valve, and flow inside the pivot recesses of the SJM was rather minimal. When the leaflets swung to close, a large backflow rushed from the secondary flat through the recesses of the ADV valve (Fig. 14c), and less flow washing could be seen inside the recesses of the SJM valve (Fig. 14d). This backflow washing, combined with the leaflet ear's wiping, was seen to be essential for inhibiting flow stasis in pivoted mechanical valves. When the valve had closed, the CFD result revealed flow leakage through the recesses in both valves.

The sequential CFD result on Plane C presented two noteworthy observations: (i) continual-flow washing;

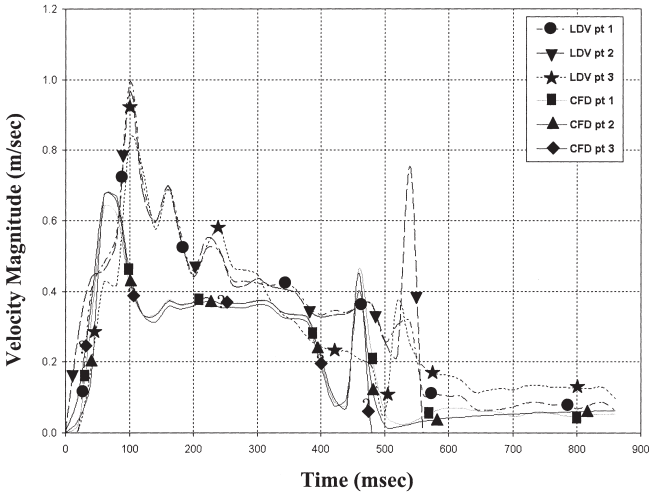

Figure 13: A typical microscopic comparison validation is shown between the velocity profiles of the LDV measurement and the CFD simulation at three selected points of the ADV valve (see Fig. 2). These profiles demonstrate general agreement between both techniques.

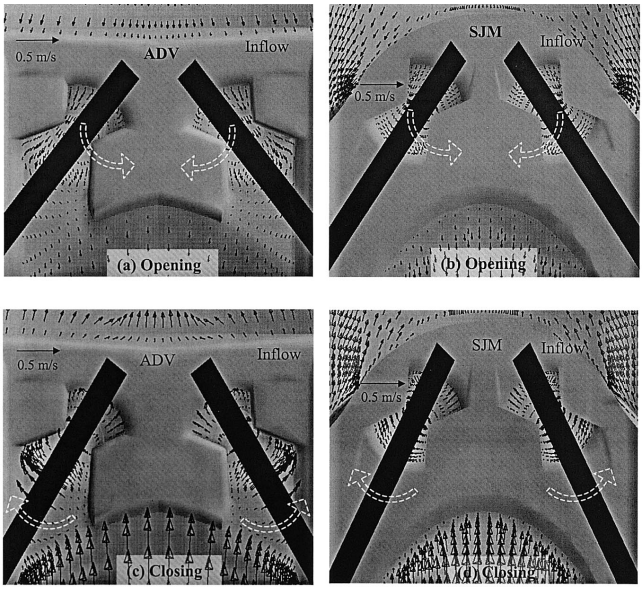

Figure 14: CFD results on Plane C show that continual-flow washing (velocity vectors) is present at the secondary flat of the ADV valve. The leaflet ears of both valves completely wipe the pivot recesses twice per cycle. This mechanical wiping completely eradicates flow structures within the recesses from cycle to cycle and prevents the development of any persistent flow stagnation.

and (ii) complete leaflet wiping. In each cardiac cycle, the secondary flat of the ADV valve accentuated the flow washing through the recess, and this observation echoed the finding in the PFV study. The CFD result showed that the leaflet movement completely eradicates velocity vectors within the pivot recess in each cardiac cycle. This periodic mechanical wiping prevented recurring microscopic flow structures and further insured the elimination of flow stasis within the pivot recesses.

LDV measurement

Typical two-component velocity vector plots on Plane C are presented in Figure 15. The velocity field in early diastole contained velocities on the order of 5-10 cm/s within the recesses of both valves (Fig. 15a and b). However, velocities on the order of 30 cm/s were observed exiting the channel created by the secondary flat of the ADV valve. In mid-diastole, flow within recesses was minimal, and consistent with the observation from the PFV and CFD simulation. When the leaflet swung to close (Fig. 15c and d), fluid backflow was seen to enter the ADV's pivot recess at a velocity of 50-60 cm/s, and the SJM's pivot recess at 50-70 cm/s. After valve closure, leakage exiting the recess persisted, with its highest velocity reaching 160 cm/s at a localized site for both valves.

Turbulent shear stresses measured in the pivots of the ADV and SJM were comparable. The maximum turbulent shear stress was observed after the valve had closed, and its magnitude was <1,000 dynes/cm^2. This was well below the reported turbulent shear stress of 4,000 dynes/cm^2 necessary to create hemolysis of blood elements (15).

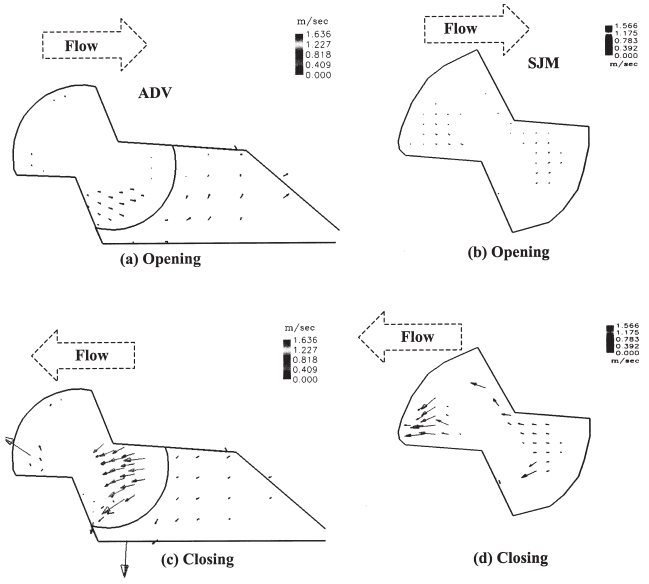

Figure 15: Schematic diagrams presenting typical LDV results on Plane C. The LDV measurement indicates continuous-flow washing through the secondary flat of the ADV in an entire cardiac cycle. The blank areas in the pivots of these plots are due to lack of LDV measurement rather than to lack of flow.

Discussion

This report introduces for the first time the application of an integrated macro/micro approach in the development of a new bileaflet mechanical valve. In this approach, the macroscopic hydrodynamic performance assessment provides an overall view of the dynamic behavior of the valve. The microscopic flow analysis reveals a detailed picture of flow properties in the pivot region, and suggests how differences in valve design can influence local flow in the critical pivot region of bileaflet valves.

The macroscopic assessment demonstrated hydrodynamic similarity between the ADV and SJM valves. This was to be expected, as both valves, on a macro scale, are bileaflet valves in which two PyC leaflets are retained in a PyC valve housing. Both valves also have similar opening angles (86° for the ADV, 85° for the SJM) and similar internal diameters.

The microscopic flow analysis explores flow properties in the pivot region that is otherwise inaccessible by a macroscopic approach and clinical evaluation standards. The analysis employs a combination of three techniques - PFV, CFD and LDV - each of which can determine microscopic flow structures within the pivot region, with certain limitations. The PFV can capture two-dimensional flow images at a pivot, but its result provides only qualitative information. The LDV can accurately measure point velocities within a pivot, but the number of points is limited due to the restricted access to this small region. The CFD can mathematically simulate and reconstruct a pivot flow domain, but the simulation depends upon known boundary conditions. Full characterization of the flow within a pivot requires the combination of these three techniques. Together, the three can mutually compensate for their individual limitations. Using only one or two techniques without cross-validation may not provide a complete picture of flow characteristics within a pivot.

The results of the current study highlight the importance of continuous-flow washing and periodic mechanical wiping in the pivot regions to prevent persistent flow stasis. These events are crucial, as flow stasis is a dominant factor in thrombus formation (16-18). For a bileaflet mechanical valve, flow washing and leaflet ear wiping depend on the valve pivot design and how the leaflet ear and pivot recess mate. The

J Heart Valve Dis
Vol. 12. No. 4
July 2003

ADV valve, with its smooth-edged bi-level butterfly pivot design, tends to facilitate increased pivot flow washing as compared to the SJM. With their leaflet ears closely mated to their pivot recesses, both the ADV and the SJM valves allow thorough mechanical wiping of the pivot regions.

The PyC structural components of the ADV valve are identical for both mitral and aortic valves. The same is true for the SJM valve. Although this integrated macro/micro approach was conducted only at the mitral position and with a single hydrodynamic setting, it is hypothesized that the flow features described above will also be present at the aortic position and under the full range of physiological hydrodynamic conditions. Altering hydrodynamic settings - for example cardiac outputs or cardiac rhythms - should not affect the basic flow characteristics through the pivots.

In summary, the crucial role of the pivot mechanism in the success of a bileaflet prosthetic valve underlines the importance of developing a new methodology to evaluate pivot flow characteristics. The current study employed an integrated macro/micro approach to evaluate the ADV valve design during its design process, using the SJM valve as a reference. The techniques used in the integrated macro/micro approach detected pivot flow structures and characteristics, such as vena contractas, flow recirculation zones, small vortices, continuous-flow washing and the absence of persistent flow stases. It is theorized that the application of this approach during the design process of a bileaflet mechanical valve can eliminate the persistent flow stases that lead to thrombus formation.

Acknowledgements

The authors thank Dave Custer, Susan Ruff and Chris Coppin for reviewing this manuscript and providing valuable comments and suggestions. The CFD simulation was performed by Adaptive-Research in California and funded by Medtronic. The LDV measurements were conducted by Georgia Institute of Technology in Georgia and funded by Medtronic.

References

1. Bodnar E. Editorial: The Medtronic Parallel valve and the lessons learned. J Heart Valve Dis 1996;5:572-573
2. Gross JM, Shu MCS, Dai FF, Ellis J, Yoganathan AP. A microstructural flow analysis within a bileaflet mechanical heart valve hinge. J Heart Valve Dis 1996;5:581-590
3. Ellis JT, Healy TM, Fontaine AA, Saxena R, Yoganathan AP. Velocity measurements and flow patterns within the pivot region of a Medtronic Parallel bileaflet mechanical valve with clear housing. J Heart Valve Dis 1996;5:591-599
4. Gao ZB, Hosein N, Dai FF, Hwang NHC. Pressure and flow fields in the pivot region of bileaflet mechanical heart valves. J Heart Valve Dis 1999;8:197-205
5. Emery RW, Nicoloff DM. St. Jude Medical cardiac valve prosthesis. J Thorac Cardiovasc Surg 1979;78:269-276
6. Klawitter JJ. Design and in vitro testing of the Duromedics bileaflet valve. First International Hemex Symposium on the Duromedics Bileaflet Valve. Austin Hemex Scientific Inc., 1985:73-81
7. Ihlen H, Molstad P, Simonsen S, et al. Hemodynamic evaluation of the CarboMedics prosthetic heart valve in the aortic position: Comparison of noninvasive and invasive techniques. Am Heart J 1992;123:151-159
8. Vallana F, Rinaldi S, Galletti PM, Nguyen A, Piwnica A. Pivot design in bileaflet valves. J Am Soc Artif Intern Organs 1992;38:M600-M606
9. Westaby S, Van Nooten G, Sharif H, Pillai R, Caes F. Valve replacement with the ATS open pivot bileaflet prosthesis. Eur J Cardiothorac Surg 1996;10:660-665
10. Replacement Heart Valve Guidance (Draft), Division of Cardiovascular, Respiratory, and Neurological Devices, United States Department of Health and Human Services, October 14, 1994
11. ISO 5840: 1996 Cardiovascular Implants - Cardiac Valve Prostheses
12. Abdullah SA, Shu CS, Hwang NHC. Dynamic performance of heart valve prostheses and testing loop characteristics. Am Soc Artif Intern Organs Trans 1983;29:296-300
13. Reul H. Cardiovascular simulation models. Life support systems 1984;2:77-98
14. Gross JM, Shermer CD, Hwang NHC. Vortex shedding in bileaflet heart valve prostheses. Am Soc Artif Intern Organs Trans 1988;34:845-850
15. Sallam A, Hwang NHC. Human red blood cell hemolysis in a turbulent shear flow: Contributions of Reynolds shear stresses. Biorheology 1984;21:783-797
16. Christy JRE, Macleod N. The role of stasis in the clotting of blood and milk flows around solid objects. Cardiovasc Res 1989;23:949-959
17. Beppu S. Hypercoagulability in the left atrium: Part I: Echocardiography. J Heart Valve Dis 1993;2:18-24
18. Yasaka M, Beppu S. Hypercoagulability in the left atrium: Part II: Echocardiography. J Heart Valve Dis 1993;2:25-34